

Evaluation of the Adhesion and Slurry Wear Erosion of Nb₂O₅ Coatings Applied by Flame Spray



MARIA JÚLIA XAVIER BELÉM, HIPÓLITO CARVAJAL FALS,
ANGEL SANCHEZ ROCA, and CARLOS ROBERTO CAMELLO LIMA

Niobium pentoxide (Nb₂O₅) has excellent chemical and thermodynamic stabilities, characteristics that have accelerated the applications of this material in the form of coatings to protect against corrosive processes. However, few studies have evaluated its performance in wear protection applications. In this research, the slurry wear erosion resistance of Nb₂O₅ coatings deposited by flame spray was studied. The microstructural characterization of the coatings was performed by optical microscopy and scanning electron microscopy (SEM) assisted by chemical analysis by energy dispersive X-ray spectroscopy (EDS). Adhesion of the coatings was determined by the adhesion test (ASTM C633-13). Image analysis was used for the quantitative study of the adhesion tested areas and porosity of the coatings. Erosive wear resistance was determined using a container tribometer with erosive mixing at a particle velocity of 9.33 m/s and two particle incidence angles. The thinner coatings had fewer microstructural defects, such as pores and microcracks, and greater adhesive strength. The thicker coatings presented a cohesive failure mode. When the impact angle of the erodent particles was 90 deg, the thickness of the Nb₂O₅ coatings should not exceed 350 μm. Nb₂O₅ coatings applied by flame spray showed good resistance to slurry wear erosion, besides inherent low cost and flexibility of the process.

<https://doi.org/10.1007/s11661-019-05456-x>

© The Minerals, Metals & Materials Society and ASM International 2019

I. INTRODUCTION

INDUSTRIAL equipment operating in aggressive environments has wear as an undesirable problem, which provokes serious technical and economic consequences.^[1] The use of coatings can increase the life of components, reducing the cost of replacement and maintenance of parts. Research and development in coatings science and surface technology is driven by an increase in industry requirements for high-performance coatings at a relatively low cost. Additionally, there is an increasing regulatory pressure to reduce hazardous waste, such as hexavalent chromium and organic compound volatiles, which are eventually produced by coating processes and can generate environmental pollution.^[2]

Niobium pentoxide (Nb₂O₅) is a material that can be used as a protective coating, increasing the protection of

industrial equipment and contributing to cost reduction, thus reducing the need to repair damages caused by corrosion and wear processes.^[3] In addition to high availability, Nb₂O₅ offers health and environmental safety, as can be seen in the REACH (Registration, Evaluation, Authorization and Restriction of Chemicals) regulation, which states that this material presents no particular hazard, unlike traditional materials, such as cobalt (Co) and tungsten carbide (WC), most frequently used in the protection against wear. WC and Co give rise to a spectrum of risks and health problems caused by the formation of tungsten trioxide (WO₃) and tricobalt (Co₃O₄) tetroxide on WC and Co surfaces by oxidation or tribo-oxidation released into the environment by means of particles that are released during the wear process.^[4] WO₃ and Co₃O₄ have received classifications and labels notified under the REACH regulation with risks to human health.^[4,5] In this context, Nb₂O₅ can be considered a promising material to protect the substrate from a hostile environment, presenting economic and environmental advantages.

Nb₂O₅ has unique chemical and physical characteristics, such as high chemical stability, phase-dependent properties, and high corrosion resistance, in acidic and alkaline media,^[6,7] besides presenting electronic and optical properties, which allow its application in gas

MARIA JÚLIA XAVIER BELÉM and CARLOS ROBERTO CAMELLO LIMA are with the Production Engineering Graduate Program, Methodist University of Piracicaba, Piracicaba, SP 13451-900 Brazil. Contact e-mail: crclima@unimep.br HIPÓLITO CARVAJAL FALS and ANGEL SANCHEZ ROCA are with the College of Mechanical and Industrial Engineering, Oriente University, CP 90900 Santiago de Cuba, Cuba.

Manuscript submitted February 26, 2019.

Article published online September 25, 2019

sensors,^[8] in electrochromic devices,^[9–11] in solar cells,^[9,12,13] optical devices,^[14,15] and as catalysts.^[16]

Nb₂O₅ is one of the main niobium oxides, exhibiting resistance to corrosion and wear,^[17,18] thermodynamic stability, and biocompatibility,^[19] extending engineering applications for use as a biomaterial.^[20] Several methods of deposition can be used to obtain protective layers based on Nb₂O₅, such as sol–gel techniques,^[21] chemical vapor deposition,^[22] physical vapor deposition,^[23,24] and thermal spray.^[25]

When compared to other technologies, thermal spray generally shows lower cost, higher deposition rate, and lower environmental impact.^[2,26,27] However, thermally sprayed coatings usually have pores, which are formed during the deformation and solidification processes of the molten or semimolten droplets upon impact on the substrate, which directly influences the performance of the coating, precisely on the mechanical properties, adhesion to the substrate, and cohesion of the layers,^[28] as well as in the corrosion and wear resistance.

Considering the importance of Nb₂O₅ as an alternative coating to WC and Co-based ones, the objective of this study is to evaluate the adhesion strength and resistance to slurry wear erosion of Nb₂O₅ coatings applied by flame spray on low carbon steel substrates.

II. MATERIALS AND METHODS

A. Coatings Application and Characterization

A flame spray process was used for the application of Nb₂O₅ coatings. The spraying equipment was the TeroDyn System 2000 (Eutectic Castolin, Lausanne, Switzerland). The coating material was Nb₂O₅ powder, manufactured by CBMM (Brazilian Metallurgy and Mining Company, MG, Brazil), with 99.1 wt pct purity. The morphology and chemical composition of the powder are shown in Figure 1. The powder exhibits morphology of irregular size and shape, with a strong

tendency toward spherical formation. It is possible to observe in the augmented detail small agglomerates formed in the particles with a porous surface.

The substrate material was AISI 1020 carbon steel. The substrate surface was cleaned, according to Standard 8501-1,^[29] and abrasive blasted with aluminum oxide. A bond coat of NiAl (Metco 450NS), 50- μ m thick, was applied by flame spray previously to the top coat application. The parameters of the spray process used for both bond coat and top coat application are shown in Table I.

Coatings with thicknesses of 350 and 550 μ m were applied and the microstructure was analyzed by scanning electron microscopy (SEM) using a Zeiss microscope model EVO MA15. Analyses of the chemical composition of the samples were performed at specific points of the microstructure by energy dispersive X-ray spectroscopy (EDS).

Six microhardness measurements were performed along the cross section of the coating, from top to substrate, using a Shimadzu microdurometer (model HMV 2T) with a load of 50 g (HV_{0.05}). The porosity of the cross sections of the coatings (Nb₂O₅ + NiAl) was analyzed using the image analysis technique.^[30] The methodology to perform the analysis consisted of digital processing of the microstructural images (SEM) to characterize the pores and their distribution within the coating. Initially, the images were converted into binary images (w/b). To evaluate the percentage of the pore area within the coating, the area relative to the coating was selected in the binary image. The analysis allowed obtaining the areas of the pores, their percentage inside the coating, and the statistical deviations and averages.

B. Adhesion Test

The Tensile Adhesion Test followed the ASTM C633-13 standard.^[31] Five coated specimens were used for each thickness. For the bonding of the cylindrical

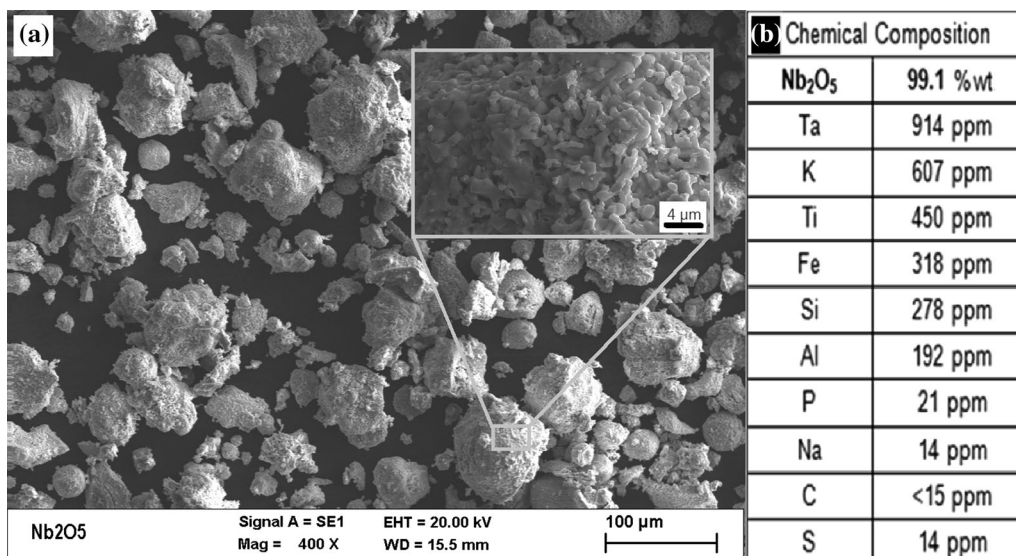


Fig. 1—Nb₂O₅ powder: (a) general morphology and (b) chemical composition.

test specimens and counterparts in AISI 1020 steel, an epoxy adhesive Scotch Weld DP-460 (3M) with a nominal shear strength of 31 MPa was used. The test pieces joined with the adhesive were positioned on a holder to assist the joint step and mounted to the tensile compensation device, as shown in Figure 2. The curing time of the epoxy adhesive was 48 hours in air.

The tensile adhesion tests were performed on a universal machine, model EMIC 23-20, with a nominal capacity of 20 kN (2000 kgf). A nominal load of 15 kN and a displacement rate of 0.02 mm/s were applied. After the failure of the joints, the surfaces of the coated specimens and related counterparts were analyzed and the fracture region was evaluated by image analysis. The areas tested and the failure modes for each thickness were determined and characterized. To define the adhesive/cohesive strength of the samples, the maximum supported strength was divided by the cross-sectional area of the specimen as specified in the reference standard.

C. Slurry Wear Erosion Test

Five samples of 15 mm × 22 mm were prepared for the slurry erosion test. A mixing vessel-type tribometer (laboratory version) was used, as shown in Figure 3. Quartz sand (SiO₂), with a particle size of 300/420 μm, was used as abrasive particles. The erosive mixture consists of 700 g of distilled water and 300 g of SiO₂. The samples were embedded in a stainless steel sample

holder, which allows variation of the impact angle of the erodent (30 or 90 deg). The impact velocity of the particles was kept constant at 9.33 m/s.

Preliminary tests were performed to examine whether the coatings were not being fully removed during erosion. Thus, the total duration of the assay was set at 1 hour to avoid the substrates becoming unprotected.

Four samples of each coating thickness of Nb₂O₅ were used for the erosion test at a velocity of 9.33 m/s and angle of impact of 30 deg. The same procedure was performed with four more specimens for each thickness of the coating, but the angle of impact was changed to 90 deg. Mass loss analyses due to a partial loss of the coating were done after a 1-hour run of the test by visual inspection, scale weighing, and chemical surface examination after erosion.

After each hour of testing, the specimens were removed from the device, washed, removed from moisture using pure acetone, dried, and weighed using a Shimadzu digital scale (model AY220). With this, the mass loss for each test was evaluated. Then, the results were normalized to volume loss, according to Eq. [1], using the density of Nb₂O₅ (4.95 g/cm³).

$$V_1 = \frac{M_l(\text{g})}{d(\text{g}/\text{cm}^3)} \times 1000 \text{ cm}^3 \quad [1]$$

In Eq. [1], V_1 is the volume loss (mm³), M_l is the mass loss (g), and d is the density (g/cm³).

Table I. Parameters Used in the Spraying of the Bond Coat and Nb₂O₅ Coating

Feed Rate	Spray Distance	Oxygen Pressure	Acetylene Pressure	Compressed Air	Spray Speed
25 g/min	120 mm	0.26 MPa	0.41 MPa	0.41 MPa	140 mm/s

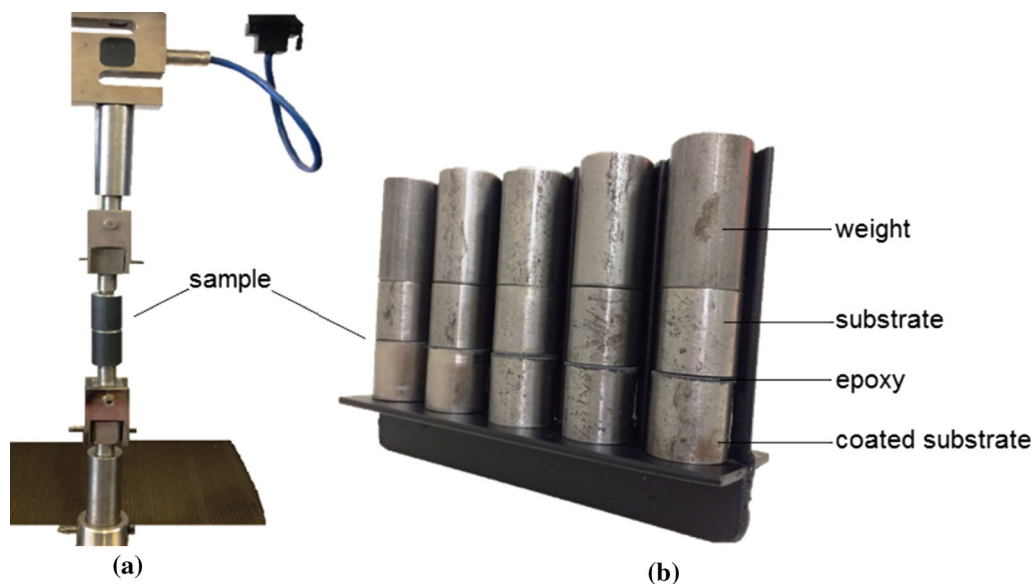


Fig. 2—(a) Compensation device for adhesion strength test. (b) Preparation of test specimens for the adhesion test according to ASTM C633-13.^[31]

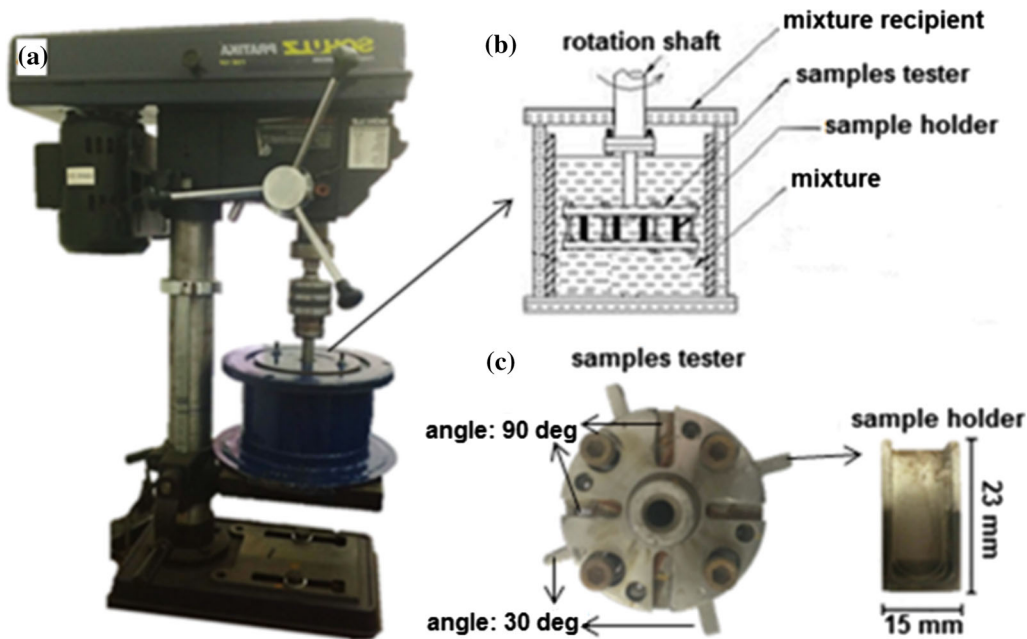


Fig. 3—(a) Mixing vessel tribometer, (b) detail of the erosive mixture container, and (c) detail of the sample holder.

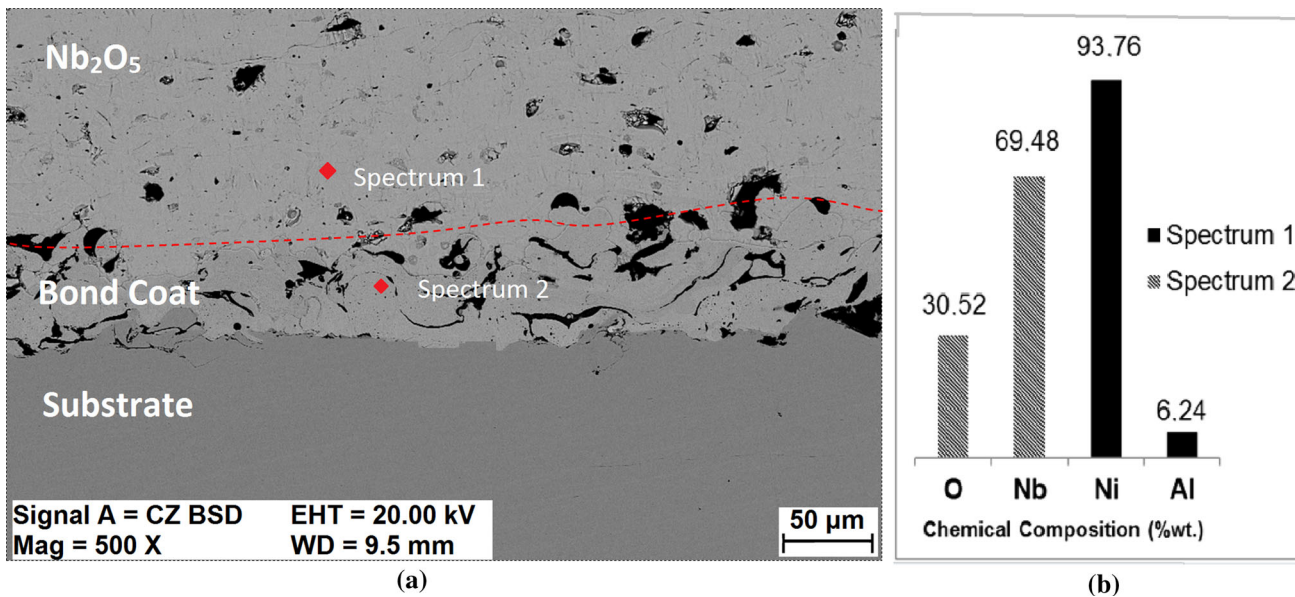


Fig. 4—Coating analysis: (a) EDS analysis region and (b) EDS results.

III. RESULTS AND DISCUSSION

From the microstructural analysis, it was possible to identify the coating formation characteristics for the two different coating thicknesses. Figure 4 shows the cross-sectional image and EDS analysis performed on the coating in both the bond and top coat regions. The presence of the Ni and Al in the bond coat (beneath the red line), as well as Nb and oxygen (that comes from the formation of oxides in the spraying process), can be observed in the EDS analysis of spectra 1 and 2, respectively. The bond coat layer reduces the stresses between the substrate and the coating and it is also

responsible for producing a rough surface for the Nb_2O_5 particles to adhere and form the coating.^[32]

The bond coat formed a lamellar structure, as can be seen in Figure 4, with the presence of elongated pores, which are formed by the voids between splats. After the bond coat application, subsequent layers of Nb_2O_5 were deposited, forming coatings with 350- and 550- μm thicknesses, as shown in the cross-sectional images of the as-sprayed coatings in Figure 5. The porosity present in the coatings was evaluated by the image analysis technique through SEM micrographs, allowing characterization of the number of pores and their

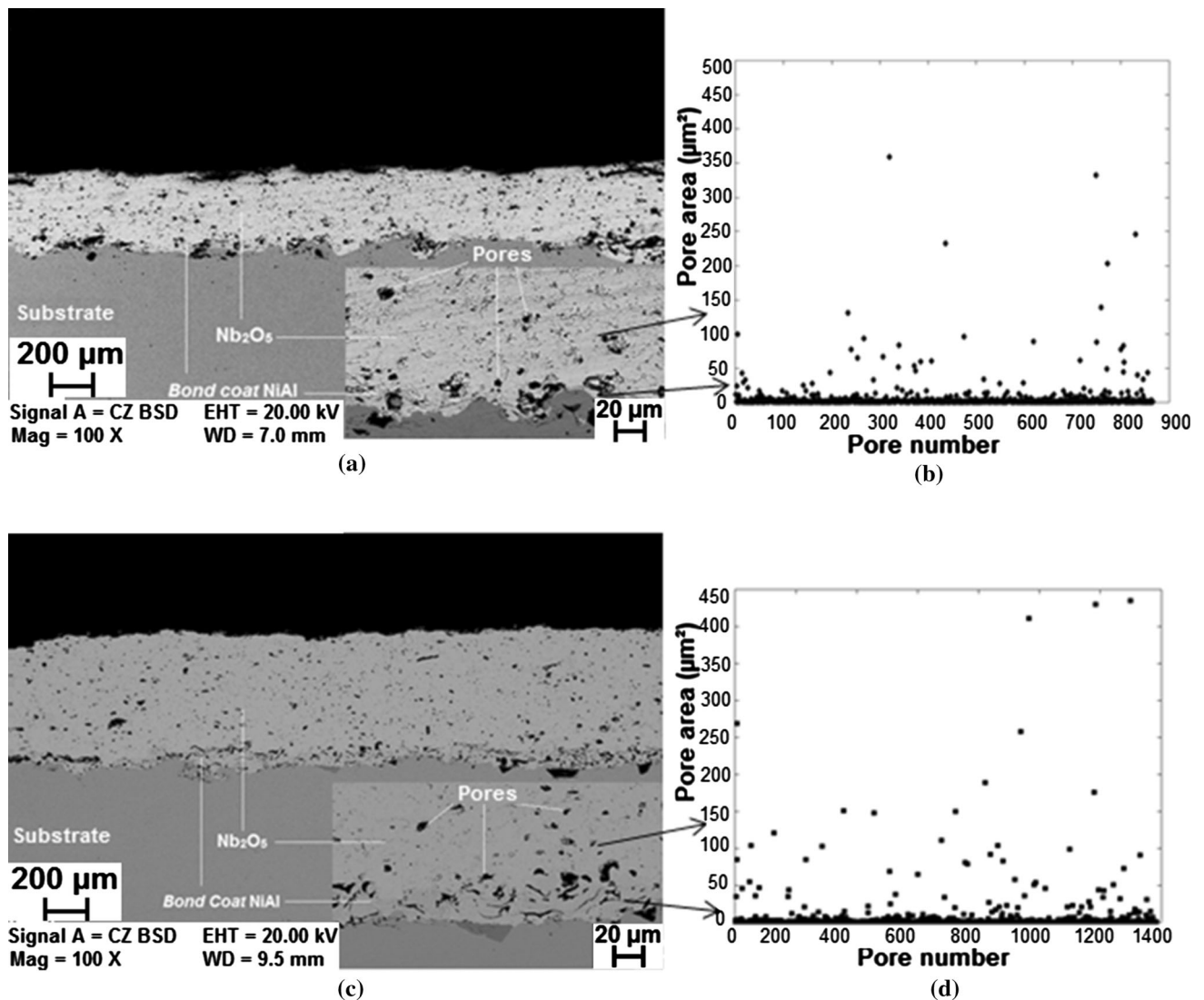


Fig. 5—Nb₂O₅ as-sprayed coatings: (a) and (b) thickness of 350 μm, number of pores per area; (c) and (d) thickness of 550 μm, number of pores per area.

distribution within the coating, as shown in the graphs of Figures 5(b) and (d).

The mean pore percentages were 3.8 and 4.2 pct for the 350- and 550-μm coatings, respectively. These porosities are in the range of those obtained for WC10Co4Cr and Cr₃C₂NiCr coatings applied by flame spray, which presented porosities of 0.26 and 6.93 pct, respectively.^[33]

Globular pores were formed in the spraying process, which extended throughout the microstructure of the Nb₂O₅ coatings; an intensification of this type of pore was observed for increasing thicknesses. Correspondingly, elongated pores are formed between the lamellae, and the presence of partially molten particles, microcracks, and oxides can be observed, as pointed out in Figure 6.

The pores generally presented areas below 50 μm, as can be seen in Figure 5 for both coatings. Larger and elongated pores were observed in the bond coat layer, as shown in Figure 7, regardless of the thickness of the

coating. This is an important aspect because the defects, such as pores and microcracks, can directly interfere in the results of adhesion and wear tests.

A. Microhardness

The microhardness values (HV_{0.05}) of the Nb₂O₅ coating measured in the cross section of the coatings are shown in Table II.

The different microhardness values within the same coating were caused by the microstructural heterogeneity of these coatings due to the presence of oxides, partially molten particles, and pores, as shown in Figure 5. The microhardness values varied with the thickness change. The 350-μm coating presented the highest individual values of the microhardness, with a mean of 764 HV_{0.05}. The 550-μm coating showed a mean microhardness value of 633 HV_{0.05}. The reduction of the microhardness with the increase of the coating thickness can be partially explained by the greater

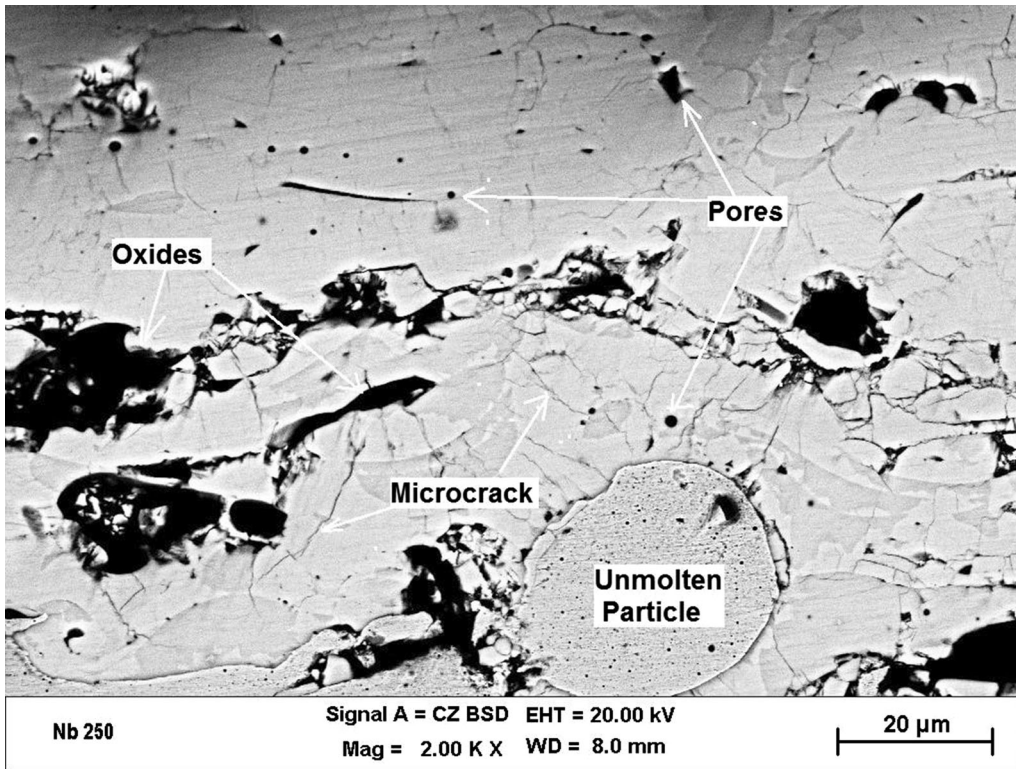


Fig. 6—SEM cross-sectional image of the Nb₂O₅ as-sprayed coating showing typical microstructural defects.

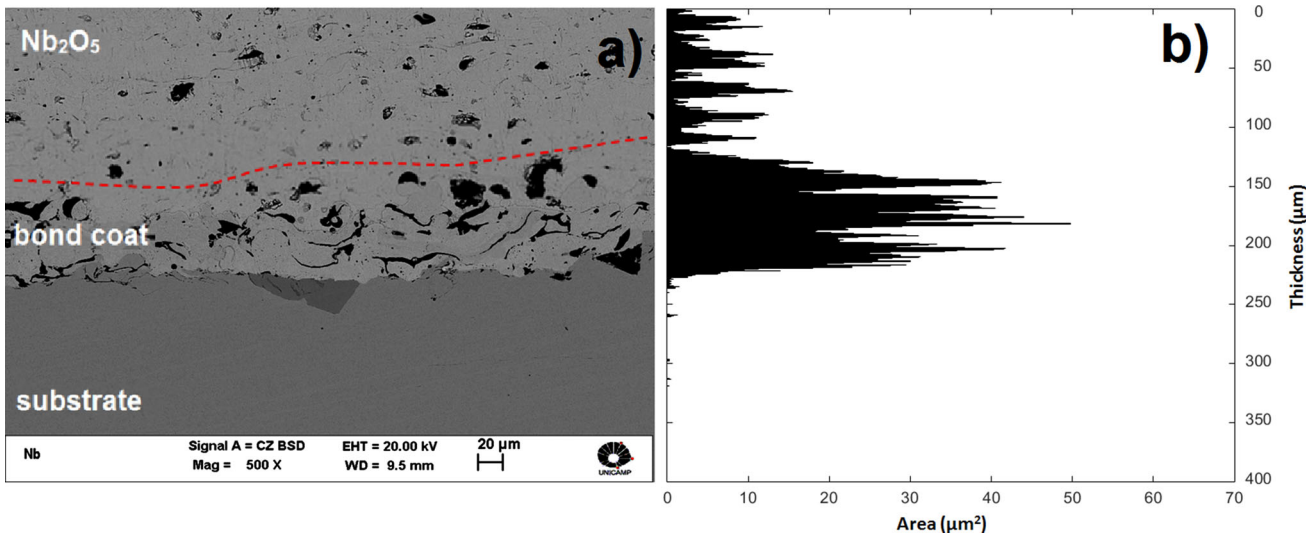


Fig. 7—(a) Cross-sectional image of the 550- μm Nb₂O₅ coating; (b) distribution of the pore areas in the thickness of the coating. The dotted red line delimits the bond coat/top coat interface (Color figure online).

quantity of pores present in the microstructure of greater thickness. As a comparison, very fine Nb₂O₅ layers obtained through the magnetron sputtering and dual ion beam sputtering deposition processes presented lower microhardnesses than the coatings obtained in this study (< 612 HV).^[34,35]

Microhardness is one of the important properties for wear resistant coatings. Nb₂O₅ is generally not used in

mechanical applications due to its relatively low hardness.^[36] However, hardness should not be the only criterion for choosing wear resistant materials. The type of load that the material is subject to, as well as the abrasive/erosive particles present in the working environment, the impact angle of these particles, combinations with other degradation processes, and environmental aspects, among other factors, must be considered.

Table II. Microhardness (HV_{0.05}) Results of Nb₂O₅ Coatings

Thickness (μm)	Measurements						Average	Standard Deviation
	1	2	3	4	5	6		
350	612	834	775	803	879	680	764	99
550	551	625	581	727	571	740	633	82

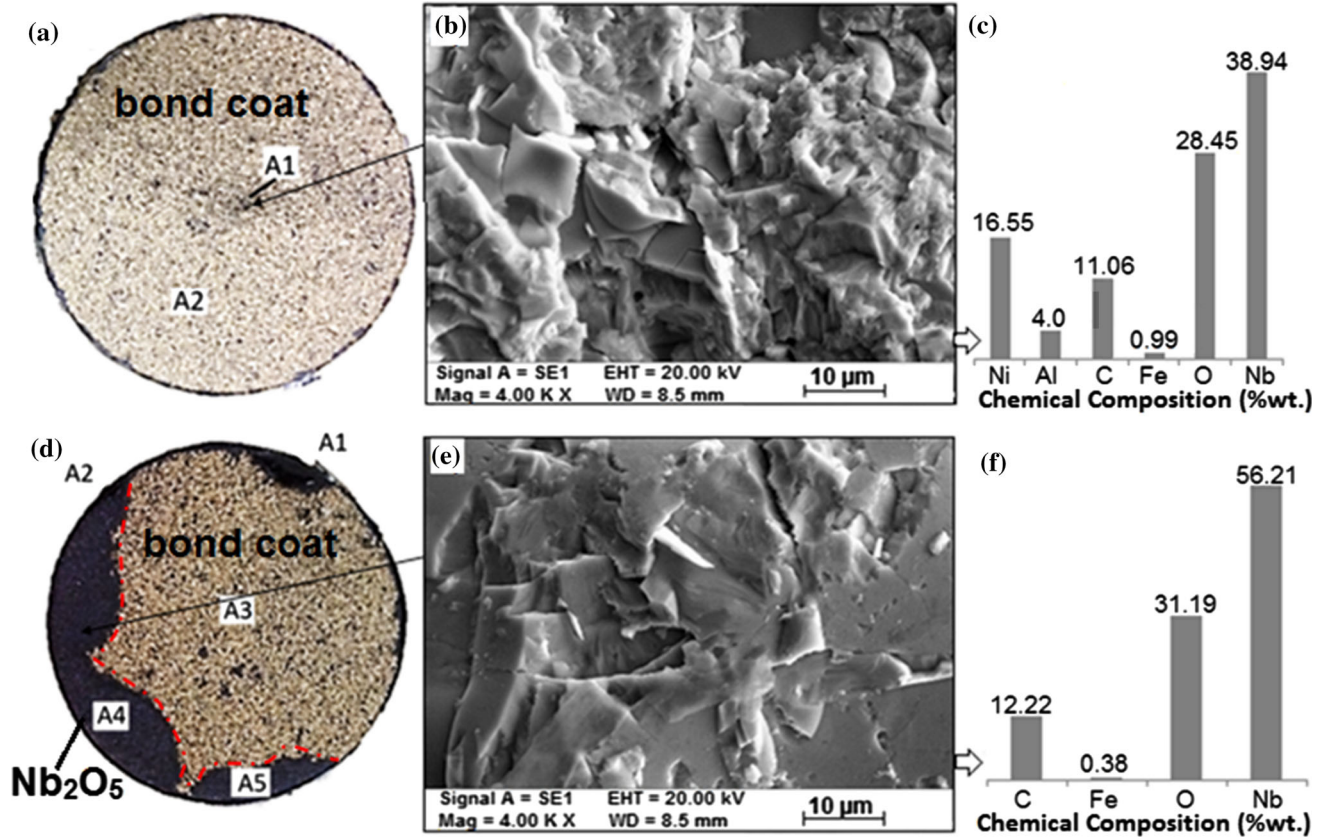


Fig. 8—Coating analysis: (a) to (c) fracture in the 350-μm coated cylinder, fracture macrography, and EDS result; (d) to (f) fracture in the 550-μm coated cylinder, fracture macrography, and EDS result.

B. Tensile Adhesion Test

The adhesion of the coatings to the substrate was measured following the ASTM C633-13 standard. The coating with a thickness of 350 μm had higher tensile strength, with a mean value of 15.27 ± 0.91 MPa. The 550-μm coating had a mean stress of 13.49 ± 0.97 MPa up to rupture, with lower adhesive strength. Therefore, the adhesion of the coatings was inversely proportional to the increase in the thickness of the layers.

ASTM C633-13^[31] presents the following failure modes of coatings obtained by thermal spraying: cohesive (when it occurs at the glue interface with the top coating or inside the coating), internal adhesive (when it occurs at the glue interface with the bond coat), and adhesive (when it occurs at the bond coat interface with the substrate or inside the bond coat). The results of the failure mode analysis are presented in Figure 8,

indicating the fracture region and the chemical composition obtained by EDS.

It can be seen in Figure 8(a) that the 350-μm coating had 0.33 pct of cohesive failure mode (A1) and most, 99.67 pct, of internal adhesive failure mode, which is the interface fracture of the bond coat with the coating (A2); this type of failure is preferred in coatings applied by thermal spray, according to ASTM C633-13. The coating with a thickness of 550 μm showed regions with fracture inside the coating (Figure 8(d)), corresponding to 25.94 pct of cohesive failure mode (represented by the sum of areas A1, A2, A4, and A5), and fracture of 74.06 pct at the bond coat interface coating, which is internal adhesive failure mode (A3). This means that the increased thickness increased the porosity and, as a result, there was a higher percentage of fracture between splats (interlamellar fracture).

Per Varavallo *et al.*,^[37] cohesive failures should be avoided to ensure efficient application of a coating. Studies are needed on the variables involved in cohesive failure to eliminate them from the process. Still, according to the authors, one way to minimize the cohesive failure is reducing the thickness of the layer, as the ideal layer thickness would be one where the fracture is of the internal type of adhesive (coating/bond coat).

C. Slurry Wear Erosion Test

The slurry wear erosion test was performed with angles of incidence of the particles of 30 and 90 deg, at a speed of 9.33 m/s. The wear resistance was evaluated by the mass loss of the tested samples and then normalized to volume loss. The results of the mean values of volumetric wear loss are shown in the graph of Figure 9.

In Figure 9, it can be seen, in general, that the volumetric loss was lower for the impact angle of the erodent of 30 deg, regardless of coating thickness. However, in this condition, the lowest volumetric loss ($13.01 \pm 2.17 \text{ mm}^3$) was obtained for the coating thickness of $550 \mu\text{m}$. When the angle of impact of the erodent was 90 deg, the thinner coating ($350 \mu\text{m}$) had the lowest volume loss ($26.50 \pm 1.86 \text{ mm}^3$), while the $550\text{-}\mu\text{m}$ coating had, in this condition, the highest volumetric loss, $33.25 \pm 2.6 \text{ mm}^3$.

The erosive wear resistance of Nb_2O_5 coatings was lower when compared to the coatings of WC10Co4Cr and $\text{Cr}_3\text{C}_2\text{NiCr}$ applied by flame spray, which presented losses of 29.99 and 21.84 mm^3 , respectively, in the same kind of test,^[33] lower than the value verified for Nb_2O_5 coatings, which was 33.25 mm^3 .

The voids formed between the lamellae during the impact of the molten material or partially during the spraying caused the Nb_2O_5 layers to exhibit less cohesion in the condition of the studied wear. It is important that the microstructure of the coating is as

homogeneous as possible to reduce the number and size of defects that originate.^[38] Higher values of microhardness with a low deviation of these values and low porosity are some of the properties that indicate good cohesion, presenting a microstructure of homogeneous coating,^[38] which would guarantee better resistance to wear.

During the erosion, Nb_2O_5 particles were removed from the surfaces of the samples, causing crack propagation, which occurs mainly from the pores present in the microstructure leading to a high loss mass.^[39,40] However, mainly because of its high corrosion resistance associated with an adherent layer, Nb_2O_5 is considered a material with important properties for tribological applications.^[41]

It has been observed and proven that the mechanism of erosion process depends mainly on the impact angle of erosive particles when the impact velocity has remained constant. As discussed earlier, the lowest average loss rates were at a lower impact angle of 30 deg for both coating thicknesses. In brittle coatings, such as Nb_2O_5 , the main mechanism of erosive wear, by microcutting, has diminished the effect on the loss of material. When the angle of impact of the erodent was 90 deg, greater surface degradation due to wear occurred in the material; in this case, the particles impact perpendicular to the brittle coating, causing the formation of fatigue microcracks, pulling out more material, and, consequently, generating greater volumetric losses.

The $550\text{-}\mu\text{m}$ -thick Nb_2O_5 coating presented higher amounts of pores, microcracks, and other interlamellar defects in the layers, as shown in Figure 6. These defects directly influenced the lower adhesion between the lamellae and, consequently, the formation and growth of the microcracks of fatigue by impact of the erodent, as well as the loss of material with the increase of the angle in the erosion test. With a thickness of $350 \mu\text{m}$,

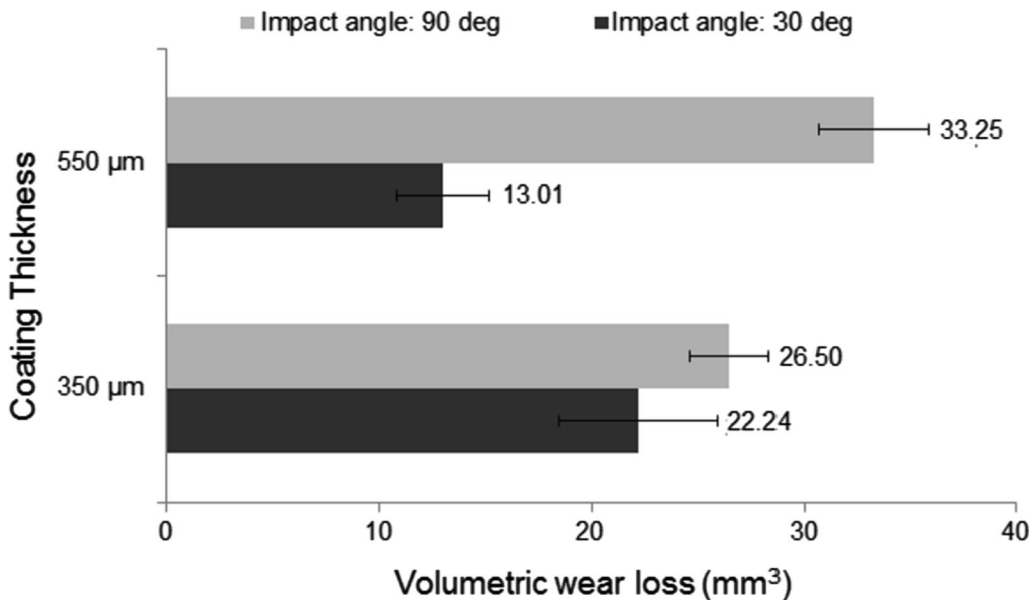


Fig. 9—Volumetric wear loss of the Nb_2O_5 coating in the erosive wear test.

Nb_2O_5 coatings have better adhesion, higher microhardness, and better wear resistance at 90 deg particle incidence angle.

In order to understand the mechanism of slurry wear erosion of the Nb_2O_5 coatings, the worn surfaces were analyzed by MEV. Figure 10 shows the worn surfaces of coatings at the impact angles of 30 deg (Figure 10(a)) and 90 deg (Figure 10(c)). At the low impact angle, the erodent caused microcutting and small areas of brittle fracture; it is also possible to observe abrasion marks in Figure 10(a). It is seen in Figure 9(b), for the normal impact angle (90 deg), that the coating has been fatigued due to the repeated impact of the erodent particles. Fracture in the Nb_2O_5 lamellae resulted in material loss due to the fragile mode of microfractures.

The main failure modes observed in the coatings were erosion by brittle fracture, plastic deformation, and removal of the ductile bond coat. Similar failure modes were observed in cermet coatings,^[42] demonstrating the similar characteristics of Nb_2O_5 with ceramic phases.

The fragile fracture of the ceramic phase is predominant for cermets in erosion due to the transmission and accumulation of impact energy.^[43] The microcracks formed in the subsurface of the coatings tend to propagate induced by the high speeds, causing greater removal of the material, especially at the edges of the exposed coatings. The fragility present in the layers significantly decreases the plasticity of the cermet or

similar materials, which leads to a decrease in erosion resistance.^[42] The Nb_2O_5 coating, despite showing good adhesion, requires special care in the application process. It is necessary to optimize the spraying parameters or even change the thermal spray technique in order to improve the flow and impact of the splats onto the substrate to obtain a denser layer with fewer defects. A good interfacial bonding of the bond coat with the coating, in addition to high values of microhardness, results in better behavior when subjected to wear.^[44]

To verify the Nb_2O_5 layers in relation to the removal of the coating after erosion, analyses of the surface chemical compositions were performed by X-ray fluorescence spectrometry (FRX). It was verified that the protective layer still remained in the substrate after the erosion test even for the impact angle of greater aggressiveness, as shown in Figure 11. The higher Nb content confirms the presence of the coating layer for both thicknesses.

The 550- μm coating showed a higher mass loss at a 90 deg impact angle. However, the surface still exhibited niobium oxide at the end of the test (Figure 11(a)), meaning that the coating was still there. In the same way, at the greater impact angle of the particles, the 350- μm coating better supported the erosion test (Figure 11(b)). The 350- μm coating showed higher microhardness, which theoretically helps to retain integrity and then prevent the coating from moving

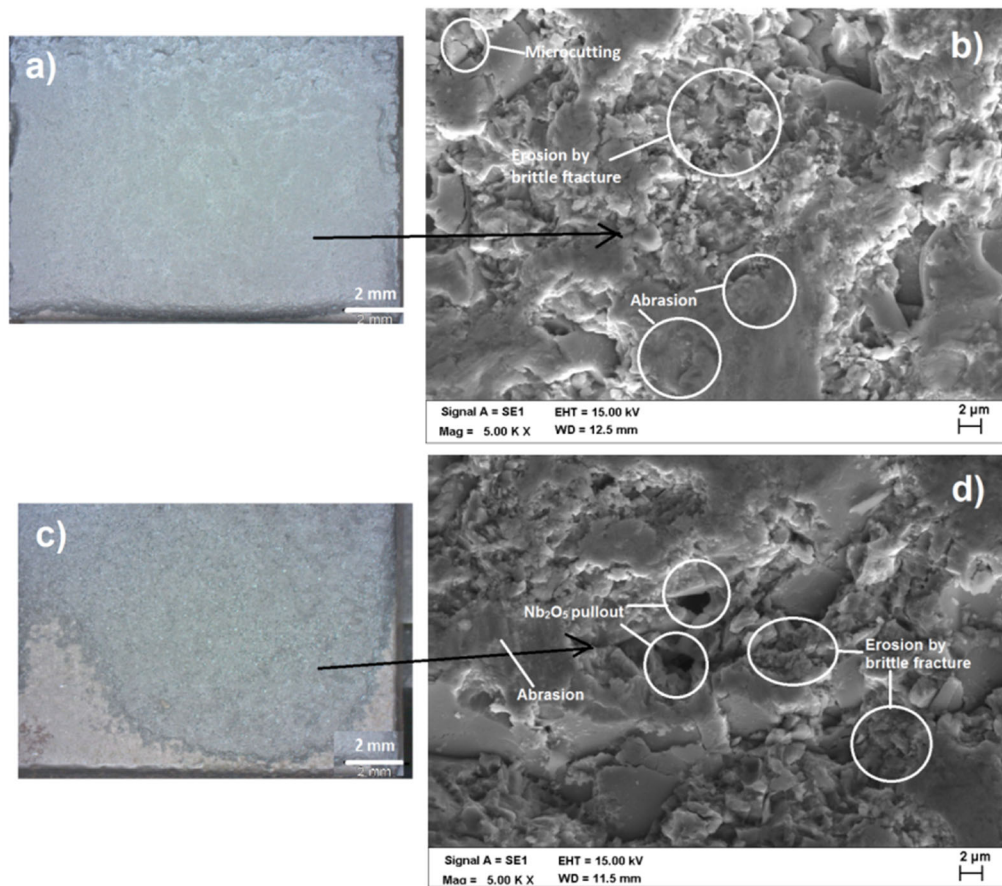


Fig. 10—Worn surfaces and wear mechanisms of Nb_2O_5 flame-sprayed coatings for impact angles of (a) and (b) 30 deg and (c) and (d) 90 deg.

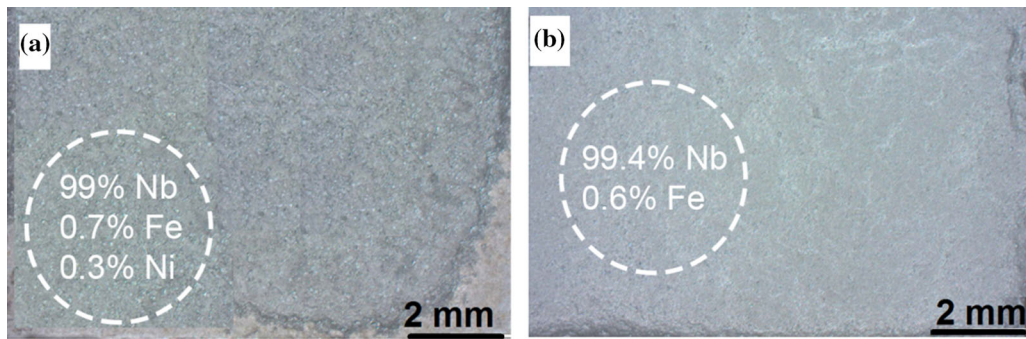


Fig. 11—Surface of the coatings after erosion at 90 deg impact angle: (a) 550 μm and (b) 350 μm showing the results of FRX.

under the impact of the erosive particles.^[45] However, for the thicker coating, the impact energy was also transmitted to the bond coating, and because of this energy accumulation, the cracks propagated throughout the layer, especially at the exposed edges. Thus, the coating began to wear with greater intensity, leading to increased loss of material related to the weak splats interface.

IV. CONCLUSIONS

Dense Nb_2O_5 coatings with good adhesive strength were obtained by flame spray. The porosities of 3.8 and 4.2 pct correspond to the typical values of coatings applied by the low velocity flame spray process.

The microhardness values varied according to the thickness change. The 350- μm -thick coating had a higher average microhardness of 764 $\text{HV}_{0.05}$, which was influenced by the lower number of pores, oxides, and microcracks present in the layers.

The thinner coatings presented higher adhesion strength, with a mean value of 15.27 MPa, which showed a higher rate of internal adhesive failure mode. With the increase of the thickness to 550 μm , the adhesion strength decreased, evidenced by the presence of the cohesive failure mode.

The thickness of the coatings and the angle of impact of the erodent influenced the resistance to erosive wear. The lower erosive wear resistance of Nb_2O_5 coating was presented at a 90 deg angle and for a thickness of 550 μm .

In spite of showing lower resistance to erosive wear than WC coatings, the Nb_2O_5 coatings applied by flame spray processes can be attractive for industrial applications, due to the low cost and flexibility of the process in addition to the good resistance to erosive wear.

ACKNOWLEDGMENTS

One of the authors (MJXB) appreciates the financial support from CAPES, Brazil. CRCL and HCF acknowledge the support of the São Paulo Research Foundation (FAPESP), Grant No. 2017/25363-0.

Special acknowledgement is due to Mr. Flávio Camargo, OPT Brazil, for technical assistance. This work was partially supported by the Program FAP - UNIMEP, Grant No. FAP119/17.

REFERENCES

1. K. Holmberg, P. Kivikytö-Reponen, P. Härkisaari, K. Valtonen, and E. Erdemir: *Tribol. Int.*, 2017, vol. 115, pp. 116–39.
2. *Nanocoatings and Ultra-Thin Films: Technologies and Applications*, 1st ed., A.S.H. Makhlof, and I. Tiginyanu, eds., *Nanocoatings and Ultra-Thin Films: Technologies and Applications*, 1st ed., Woodhead Publishing Limited, Cambridge, 2011.
3. M.R. Ripoll, N. Ojala, C. Katsich, V. Totolin, C. Tomastik, and K. Hradil: *Mater. Des.*, 2016, vol. 99, pp. 509–20.
4. M. Woydt, H. Mohrbacher, J. Vleugels, and S. Huang: *Met. Powder Rep.*, 2016, vol. 71 (4), pp. 265–72.
5. M. Woydt, S. Huang, J. Vleugels, H. Mohrbacher, and E. Cannizza: *Int. J. Refract. Met. Hard Mater.*, 2018, vol. 72, pp. 380–87.
6. F. Idrees, J. Hou, C. Cao, F.K. Butt, I. Shakir, M. Tahir, and F. Idrees: *Electrochim. Acta*, 2016, vol. 216, pp. 332–38.
7. R.A. Rani, A.S. Zoolfakar, J.Z. Ou, M.R. Field, M. Austin, and K. Kalantar-Zadeh: *J. Mater. Chem. A*, 2014, vol. 2 (38), pp. 15683–15703.
8. R.A. Rani, A.S. Zoolfakar, J.Z. Ou, M.R. Field, M. Austin, and K. Kalantar-Zadeh: *Sens. Actuator B*, 2013, vol. 176, pp. 149–56.
9. M.A. Aegerter: *Sol. Energy Mater. Sol. Cells*, 2001, vol. 68 (3–4), pp. 401–22.
10. C.O. Avellaneda, A. Pawlicka, and M.A. Aegerter: *J. Mater. Sci.*, 1998, vol. 33 (8), pp. 2181–85.
11. T. Maruyama and S. Arai: *Appl. Phys. Lett.*, 1993, vol. 63 (7), pp. 869–70.
12. E. Barea, X. Xu, V. González-Pedro, T. Ripollés-Sanchis, F. Fabregat-Santiago, and J. Bisquert: *Energy Environ. Sci.*, 2011, vol. 4 (9), pp. 3414–19.
13. A. Le Viet, R. Jose, M.V. Reddy, B.V.R. Chowdari, and S. Ramakrishna: *J. Phys. Chem. C*, 2010, vol. 114, pp. 21795–21800.
14. S. Sanghi, S. Sanghi, S. Rani, A. Agarwal, and V. Bhatnagar: *Mater. Chem. Phys.*, 2010, vol. 120 (2–3), pp. 381–86.
15. N. Usha, R. Sivakumar, C. Sanjeeviraja, and M. Arivanandhan: *Optik*, 2015, vol. 126 (19), pp. 1945–50.
16. D. Prasetyoko, Z. Ramli, S. Endud, and H. Nur: *Mater. Chem. Phys.*, 2005, vol. 93 (2–3), pp. 443–49.
17. M. Grobelny, M. Kalisz, M. Mazur, D. Wojcieszak, D. Kaczmarek, J. Domaradzki, M. Świniarski, and P. Mazur: *Thin Solid Films*, 2016, vol. 616, pp. 64–72.
18. M. Kalisz, M. Grobelny, M. Mazur, M. Zdrojek, D. Wojcieszak, M. Świniarski, J. Judek, and D. Kaczmarek: *Thin Solid Films*, 2015, vol. 589, pp. 356–63.
19. D. Velten, E. Eisenbarth, N. Schanne, and J. Brems: *J. Mater. Sci.*, 2004, vol. 15 (4), pp. 457–61.
20. S.A. Pauline and N. Rajendran: *Ceram. Int.*, 2017, vol. 43 (2), pp. 1731–39.

21. K.P. Premkumar, N. Duraipandy, M.S. Kiran, and N. Rajendran: *Appl. Surf. Sci.*, 2018, vol. 427, pp. 1166–81.
22. C.B. Silveira, A.F. Oliveira, S.D. Campos, E.A. Campos, and A.D. Fraportti: *Surf. Eng.*, 2012, vol. 28 (1), pp. 68–72.
23. M.F. Pillis, G.A. Geribola, G. Scheidt, E.G. Araújo, M.C.L. Oliveira, and R.A. Antunes: *Corros. Sci.*, 2016, vol. 102, pp. 317–25.
24. G. Ramírez, S.E. Rodila, S. Muhl, D. Turcio-Ortega, J.J. Olaya, M. Rivera, E. Camps, and L. Escobar-Alarcón: *J. Non Cryst. Sol.*, 2010, vol. 356 (50–51), pp. 2714–21.
25. L.R.M. Miranda, L.J. Carvalho, and A.C.G. Pereira: U.S. Patent No. 7,651,731, Jan. 26, 2010.
26. P.L. Fauchais, J.V.R. Heberlein, and M.I. Boulos: *Thermal Spray Fundamentals: From Powder to Part*, 1st ed., Springer, New York, 2014.
27. *Handbook of Thermal Spray Technology*, 1st ed., J.R. Davis, ed., *Handbook of Thermal Spray Technology*, 1st ed., ASM International, Materials Park, 2004.
28. A.S.M. Ang and C.C. Berndt: *Int. Mater. Rev.*, 2014, vol. 59 (4), pp. 179–223.
29. ISO 8501-1: 2007: Preparation of Steel Substrates before Application of Paints and Related Products—Visual Assessment of Surface Cleanliness. Part 1: Rust Grades and Preparation Grades of Uncoated Steel Substrates and of Steel Substrates after Overall Removal of Previous Coatings, International Organization for Standardization, Geneva, Switzerland, 2007.
30. S. Deshpande, A. Kulkarni, S. Sampath, and H. Herman: *Surf. Coat. Technol.*, 2004, vol. 187 (1), pp. 6–16.
31. ASTM C633-13: *Standard Test Method for Adhesion or Cohesion Strength of Thermal Spray Coatings*, ASTM International, West Conshohocken, PA, 2013.
32. G. Xanthopoulou, A. Marinou, G. Vekinis, A. Lekatou, and M. Vardavoulis: *Coatings*, 2014, vol. 4 (2), pp. 231–52.
33. M.A.R. Mojena, A.S. Roca, R.S. Zamora, M.S. Orozco, H.C. Fals, and C.R.C. Lima: *Wear*, 2017, vol. 376, pp. 557–65.
34. G. Ramírez, S.E. Rodil, S. Muhl, D. Turcio-Ortega, J.J. Olaya, D. Rivera, E. Camps, and L. Escobar-Alarcón: *J. Non Cryst. Solids*, 2010, vol. 356, pp. 2714–21.
35. E. Çetinörgü, B. Baloukas, O. Zabeida, J.E. Klemberg-Sapieha, and L. Martinu: *Appl. Opt.*, 2009, vol. 48 (23), pp. 4536–44.
36. R. Mirabal-Roja, S. Muhl, S.E. Rodil, E. Camps, M. Lejeune, and A. Zeinert: *J. Vac. Sci. Technol. A*, 2016, vol. 34 (4), p. 041305.
37. R. Varavallo, M. Manfrinato, L. Rossino, O. Maluf, and F. Camargo: *J. ASTM Int.*, 2012, vol. 9 (2), pp. 1–11.
38. V. Matikainen, S.R. Peregrina, N. Ojala, H. Koivuluoto, J. Schubert, Š. Houdková, and P. Vuoristo: *Surf. Coat. Technol.*, 2019, vol. 370, pp. 196–212.
39. C.S. Ramesha, D.S. Devaraja, R. Keshavamurthy, and B.R. Sridhar: *Wear*, 2011, vol. 271 (9–10), pp. 1365–71.
40. Z.X. Ding, Q. Wang, and Z.L. Liu: *Key Eng. Mater.*, 2008, vols. 373–374, pp. 27–30.
41. T. Oluyori, O.E. Olorunniwo, O.S.I. Fayomi, P.O. Atanda, and A.P.I. Popoola: *J. Bio Tribol. Corros.*, 2017, vol. 3 (4), p. 51.
42. W. Wan, J. Xiong, and M. Liang: *Ceram. Int.*, 2017, vol. 43 (1), pp. 944–52.
43. J. Kübarsepp, H. Klaasen, and J. Pirso: *Wear*, 2001, vol. 249 (3–4), pp. 229–34.
44. S.K. Patel, R. Nateriya, B. Kuriachen, and V.P. Singh: *Mater. Today*, 2018, vol. 5 (9), pp. 17561–71.
45. L. Zhang, Z. Huang, Y. Liu, Y. Shen, K. Li, Z. Cao, Z. Ren, and Y. Jian: *Ceram. Int.*, 2019, <https://doi.org/10.1016/j.ceramint.2019.06.221>.

Publisher's Note Springer Nature remains neutral with regard to jurisdictional claims in published maps and institutional affiliations.